A hybrid temporal LES/RANS formulation based on a two-equation subfilter model

Yacine Bentaleb, Remi Manceau

A HYBRID TEMPORAL LES/RANS FORMULATION BASED ON A TWO-EQUATION SUBFILTER MODEL

Yacine Bentaleb* **and Rémi Manceau**
Institute Pprime
CNRS–University of Poitiers–ENSMA
Poitiers, France
remi.manceau@univ-poitiers.fr

*Current address: Aeronautics Department
Imperial College London, UK
y.bentaleb@imperial.ac.uk

ABSTRACT

A novel hybrid model for statistically stationary flow simulations at moderate to high Reynolds numbers is presented. Based on a consistent formalism developed for seamless hybrid temporal LES/RANS methodologies (Fadai-Ghotbi et al., 2010b; Schiestel and Dejoan, 2005), the *Temporal Partially-Integrated Transport Model* (TPITM) approach is used to derive a two-equation subfilter model, consistent with the $k-\omega$ SST model in the RANS limit, *i.e.*, when the temporal filter width goes to infinity. Comparisons are made with a widespread hybrid RANS/LES model, the DES–SST formulation (Menter et al., 2003), which tends to the same RANS model in the RANS zones, but uses the Detached Eddy Simulation (DES) methodology to control the transition from RANS to LES. The paper discusses the features and capabilities of both approaches.

INTRODUCTION

Traditional Reynolds-Averaged Navier-Stokes (RANS) modelling is gradually replaced by hybrid RANS-LES methodologies for predicting complex turbulent flows in industrial practice. This trend has been encouraged by the increasing availability of high-performance computing, and the need of resolving unsteady phenomena at elevated Reynolds numbers. Especially, flows that entail separation from curved surfaces, featuring extremely high level of turbulence energy and shear stress in the separated shear layer, are still beyond the Large-Eddy Simulation (LES) capabilities. The standard compromise strategy is the use of "unsteady" RANS-based solution in the near-wall region, and resolved-scale motions in the rest of the domain. Some of these schemes may suffer from the absence of a theoretical formalism leading to unclear dividing line between the RANS and LES components (Gatski et al., 2007).

In the present paper, a consistant seamless hybrid temporal LES/RANS formulation based on a two-equation subfilter model is develpped. The SST RANS model is selected as the basis to derive the subfilter-stress model because of its capacity to account for the near-wall region, which is an essential point for such a hybrid modelling strategy, and because it proved reasonably accurate in aerodynamic flows with adverse pressure gradients and separation, and more generally in industrial applications (Menter et al., 2003). It is thus expected that the hybrid TLES/RANS model can be successfully incorporated into industrial and commercial codes.

A second approach is considered in this work, the DES–SST model (Menter et al., 2003). Recently, Manceau et al. (2010) has argued that, under certain conditions, an equivalence between DES and TPITM can be found. Therefore, a fair comparison is aimed herein. The two formulations are implemented into the same finite volume code, and applied to the turbulent channel flow with periodic arrangement of hill constriction, at Reynolds number 10595, for which a detailed reference database is available (Froehlich et al., 2005).

In the following, the TPITM-based modelling approach is summarised; then the key features of the DES-SST formulation is briefly presented. Finally, the results are discussed in comparison with the LES reference data.

MODELLING APPROACH

The TPITM model (Fadai-Ghotbi et al., 2010b) is derived from the exact transport equation for the Eulerian temporal energy spectrum, by integrating over frequency intervals (hence the name *partially integrated transport model*). It is the adaptation to temporal filtering of the PITM model (Schiestel and Dejoan, 2005), and is based on the introduction of two temporal filters, in order to decompose the Eulerian temporal energy spectrum into resolved scales, energetic subfilter scales and dissipative subfilter scales. This methodology enables a continuous transition from TLES to RANS, controlled by imposed variations of the temporal filter widths. The consistency of the time filtering process with the Reynolds aver-

age in the RANS limit and the formal similarity between the filtered and Reynolds-averaged equations has been adressed in detail in Fadai-Ghotbi et al. (2010b) and this development is not repeated herein.

The subfilter model

Let us denote the instantaneous velocity by u_i, the long-time averaging operator by $\overline{.}$ and the temporal filtering operator by $\langle . \rangle$. By applying the temporal filter to the Navier–Stokes equations and contracting the subfilter–scale tensor ($\tau_{ij_{SFS}}$) equation, it can be shown that, similarly to the case of spatial filtering (Germano, 1992), the transport equation of the subfilter kinetic energy k_{SFS} is formally identical to the familiar RANS equation for the total fluctuating kinetic energy k. The latter can be *exactly* decomposed ((see Fadai-Ghotbi et al., 2010b)) into the sum of a modelled part k_m and resolved part k_r as:

$$k = k_m + k_r, \quad k_m = \overline{k_{SFS}}, \quad k_r = \frac{1}{2}\left(\overline{\langle u_i \rangle \langle u_i \rangle} - \overline{u_i}\,\overline{u_i}\right) \quad (1)$$

In the present work, transport equations for k_m and $\omega_m = \overline{\omega_{SFS}}$ are derived by transforming the $k-\varepsilon$ model. Thus, the two-equation subfilter model writes:

$$\frac{Dk_m}{Dt} = P_m - C_\mu\,\omega_m\,k_m + \frac{\partial}{\partial x_j}\left[(\nu + \sigma_k\,\nu_{t_m})\,\frac{\partial k_m}{\partial x_j}\right] \quad (2)$$

$$\frac{D\omega_m}{Dt} = \gamma\frac{P_m}{\nu_{t_m}} - \beta^*\,\omega_m^2 + \frac{\partial}{\partial x_j}\left[(\nu + \sigma_\omega\,\nu_{t_m})\,\frac{\partial \omega_m}{\partial x_j}\right] + 2\,(1-F_1)\,\frac{\sigma_{\omega_2}}{\omega_m}\,\frac{\partial k_m}{\partial x_j}\,\frac{\partial \omega_m}{\partial x_j} \quad (3)$$

where

$$P_m = \tau_{ij_m}\frac{\partial \overline{u_i}}{\partial x_j} = \nu_{t_m}\left(\frac{\partial \overline{u_i}}{\partial x_j} + \frac{\partial \overline{u_j}}{\partial x_i}\right)\frac{\partial \overline{u_i}}{\partial x_j} = \nu_{t_m} S^2 \quad (4)$$

$$\nu_{t_m} = \frac{a_1\,k_m}{\max(a_1\,\omega_m, SF_2)} \quad (5)$$

and the subscript m denoting the modelled part. In order to ensure the correct RANS limit of the model, the constants appearing in the "partial" turbulent viscosity, ν_{t_m} (Eq. 5), and in the transport equations (Eqs. 2 and 3) are the same as in the SST RANS model (Menter et al., 2003), except for the β^* coefficient in the ω_m-equation, which is dependent on the temporal filter width, and ensures the transition from RANS to TLES. Note that F_1 and F_2 are the blending functions used in the original SST model, but the variables k and ω are replaced by their modelled (unresolved) contributions:

$$F_1 = \tanh(arg_1^4) \quad (6)$$

$$F_2 = \tanh(arg_2^2) \quad (7)$$

$$arg_1 = \min\left[\max\left(\frac{k_m^{1/2}}{C_\mu\,\omega_m y}, \frac{500\,\nu}{y^2\,\omega_m}\right), \frac{4\,\rho\,\sigma_{\omega_2}\,k_m}{CD_{k\omega}\,y^2}\right] \quad (8)$$

$$arg_2 = \max\left[\frac{2\,k_m^{1/2}}{C_\mu\,\omega_m y}, \frac{500\,\nu}{y^2\,\omega_m}\right] \quad (9)$$

with $CD_{k\omega} = \max\left(2\,\rho\,\sigma_{\omega_2}\,\frac{1}{\omega_m}\,\frac{\partial k_m}{\partial x_i}\,\frac{\partial \omega_m}{\partial x_i}, 10^{-20}\right)$ and y being the distance to the nearest wall.

It is found that the function β^* can be derived in a similar way to what was proposed, in the spatial filtering context, by Schiestel and Dejoan (2005) for the variable coefficient $C^*_{\varepsilon_2} = C_{\varepsilon_1} + r(C_{\varepsilon_2} - C_{\varepsilon_1})$ in the ε_m-equation, which leads to

$$\beta^* = C_\mu\,\gamma + r\,(\beta - C_\mu\,\gamma) \quad (10)$$

Alternatively, it can be deduced from a change of variables in the k–ε equations, through the relations:

$$\gamma = C_{\varepsilon_1} - 1, \quad \beta = C_\mu(C_{\varepsilon_2} - 1), \quad \beta^* = C_\mu(C^*_{\varepsilon_2} - 1) \quad (11)$$

In Eq. 10, the amount of long-time averaged modelled energy (and therefore, the amount of resolved energy), *i.e.*, the transition from TLES to RANS, is driven by the value of the energy ratio

$$r = \frac{k_m}{k} \quad (12)$$

To control effectively the energy partitioning and therefore enforce the desired behavior of the model, the above parameter has to be linked to the grid size. This issue is briefly adressed in the following section.

Dependence on the filter width

Using an equilibrium Eulerian temporal spectrum, it was shown by Fadai-Ghotbi et al. (2010b) that the energy ratio r can be related to the temporal filter width Δ_T by

$$r = \beta_0^{-1}\left(\frac{\omega_c}{C_\mu\,\omega}\right)^{-\frac{2}{3}}, \qquad \beta_0 = \frac{2}{3C_K} \simeq 0.44 \quad (13)$$

where ω_c is the cutoff frequency $\omega_c = \pi/\Delta_T$ and C_K the Kolmogorov constant. The sweeping hypothesis of Tennekes (1975) leads to using the dispersion relation $\omega = \sqrt{k}\kappa$ to link the frequency and wavenumber domains, such that the temporal filter width is related to the grid by $\Delta_T = (\Delta x \Delta y \Delta z)^{1/3}/\sqrt{k}$. The role of the coefficient β_0 is of importance since it is involved in the energy ratio r, and its effect will be investigated. In the present study, in order to enforce the RANS mode in the near-wall region ($r = 1$), as well as to better control the key parameter r, the function β^* is modified by introducing the blending function F_2 (Eqs. 7 and 9). The empirical formulation used in practice writes

$$\beta^* = C_\mu\,\gamma + \left[F_2 + (1-F_2)\,r^{observed}\right](\beta - C_\mu\,\gamma) + \min\left[\alpha\left(\frac{r^{target}}{r^{observed}} - 1\right), 0\right] \quad (14)$$

In this relation, the third term is a dynamic modification of the coefficient (Fadai-Ghotbi et al., 2010a), aiming at sustaining the correct level of resolved energy even in regions

where resolved fluctuations are not promoted by the presence of a mean shear. Thus, $r^{observed}$ is the energy ratio k_m/k, extracted from an on-the-fly averaging of the filtered fields through Eq. 1, and r^{target} is the desired energy ratio given by Eq. 13. The constant α, set to 10 in the present calculations, is influencial in the early stages of the computation only, before the statistical sampling commence. The final result is therefore independent of this parameter.

THE DES-SST FORMULATION

A second hybrid RANS/LES model is considered in this paper, based on the widely used Detached Eddy Simulation (DES) methodology. The selected underlyind RANS model is the same as in the TPITM approach. The motivation is twofold. First, as mentioned in the introduction, the SST model has shown improved capabilities in separated shear layers, combined with its robustness and industrial applicability. Second, the resulting hybrid formulation allows consistent comparison with the above TPITM based approach. The latter reason is supported by the fact that Manceau et al. (2010) has recently shown that an equivalence between DES and TPITM can be found provided that they give the same level of subfilter energy. However, the strict equivalence is not the aim of this paper. Rather, a separate investigation is conducted on the DES-SST model, focusing on its well known calibration constant, which is specific to the present flow configuration. Subsequently, a comparison of both the approaches will be presented.

Several options for the DES-limiter may be derived (Menter et al., 2003). The modification in the SST model retained here is based on the blending function F_2 (Eqs. 7 and 9). Hence, the following factor

$$F_{DES} = \max\left[\frac{L_t}{C_{des}\Delta}(1-F_2),1\right], \qquad L_t = \frac{\sqrt{k}}{C_\mu \omega} \qquad (15)$$

is introduced in the dissipation term of the k–equation, Δ being the maximum local grid spacing. In the present work, the sensitivity to the calibration constant C_{des} was carefully examined. A selection of values ranging from 0.1 to 0.6 was subjected to decaying isotropic turbulence study as well as to full computations of the present flow test case.

THE COMPUTATIONAL APPROACH

Filtered momentum and continuity equations for incompressilbe flow were solved using the finite volume based software Code_Saturne (Archambeau et al., 2004). The numerics relies on a SIMPLEC algorithm with a Rhie and Chow (1983) interpolation in the pressure correction step. As in the transport equations for the filtered momentum, the convective fluxes in the subfilter model transport equations (Eqs. 2 and 3) are approximated by second-order centred discretizations. The time-marching is based on a second-order, Crank-Nicolson scheme.

Simulations were performed with several grids of different streamwise and spanwise refinement. These are summarised in table 1. The streamwise variation of the cell dimensions along the bottom wall, normalized by the local friction velocity, are shown in Fig. 1. For the grid M1 ($160 \times 100 \times 30$), the distance of the first node off wall is $\Delta y^+/2 < 0.6$ (Fig. 1a) for both the approaches. The streamwise (Δx^+) and spanwise (Δz^+) cell dimensions are reported in Fig. 1b. Within the range $x/h = 0-5$, $\Delta x^+ < 50$ and $\Delta z^+ < 75$. With the TPITM approach, three spanwise refinements were considered (see Tab. 1). In grid M3, the spanwise cell dimension is reduced such as $\Delta z^+ < 40$ (Fig. 1c).

Statisical properties were gathered during 80 flow-through times, whose convergence was increased by averaging in the spanwise direction. Finally, the results were examined in comparison with LES reference data (Froehlich et al., 2005).

RESULTS

The separation and reattachment locations of most relevant computations are reported in Tab. 1. For the DES approach, the sensitivity study to the parameter C_{des} shows that values above 0.4 (e.g. $C_{des} = 0.5$) lead to poor predictions with excessively long separation, though less than the pure SST model (Tab. 1). It is even found that the calculations degenerate into stationary mode for $C_{des} > 0.5$, including then the standard value 0.6. Visual inspection of the structures present in the resolved field, through the isocontours of the Q–criterion shown in Fig. 2, reports on the too low resolution level with $C_{des} = 0.5$. In comparison with 0.4, only very large scale structures are obtained. Smaller values of the C_{des} constant, within the range $0.1-0.3$, were also considered and provided (statistically) a very good agreement with the reference data. However, observation of small globular structures (via the Q–criterion), confirmed by a decaying isotropic turbulence study revealed a wrong amount of energy dissipation, which is the indication that the fluctuations generated by decreasing the C_{des} parameter correspond to a white noise rather to resolved turbulence. It is found, therefore, that the optimal value corresponds to $C_{des} = 0.4$, and is retained herein for comparison purposes (labelled as DES-04 in the figures).

In the TPITM approach, two values of the key parameter β_0 are considered, 0.2 and 0.4. The latter, close to the theoretical value (0.44), leads to a lower level of the modelled part of the turbulence energy, and this is found to be necessary in the present case. In fact, $\beta_0 = 0.2$ provides similar results to SST predictions. It is worth mentioning that in the present paper, the emphasis is on the TPITM approach development. The grid refinement effect is then conveyed for this model. The grid L1 appears too coarse in the streamwise direction (too late separation and long separation) and is discarded. For $\beta_0 = 0.4$, the statistics (not included for the grids M2 and M3, except the separation and reattachment positions – Tab. 1) show that the spanwise refinement is of little consequence. The grid M1 ($160 \times 100 \times 30$) is then singled out for discussions and comparisons with the DES results and reference LES data.

The overall view of the performance of the models is conveyed in Figs. 3 – 5, which show the skin-friction coefficient, the streamwise velocity and shear-stress profiles, respectively. Using the optimal constants ($\beta_0 = 0.4$ and $C_{des} = 0.4$), the capability of both strategies to reproduce the main flow features is demonstrated, and it is observed that

Table 1: Summary of the computations; *CC*: calibration constant (β_0 in TPITM - Eq. 13 and C_{des} in DES), $(.)_s$: separation point, $(.)_r$: reattachment point.

Model	Grid	*CC*	$(x/h)_s$	$(x/h)_r$
SST	160×100 (M)	-	0.23	7.47
TPITM	$80 \times 100 \times 30$ (L1)	0.2	0.25	7.70
TPITM	$160 \times 100 \times 30$ (M1)	0.2	0.21	7.71
TPITM	$160 \times 100 \times 30$ (M1)	0.4	0.19	5.25
TPITM	$160 \times 100 \times 45$ (M2)	0.4	0.19	5.25
TPITM	$160 \times 100 \times 60$ (M3)	0.4	0.17	5.36
DES	$160 \times 100 \times 30$ (M1)	0.4	0.17	5.14
DES	$160 \times 100 \times 30$ (M1)	0.5	0.21	6.01
LES (Froehlich et al., 2005)	$196 \times 128 \times 186$	-	0.22	4.72

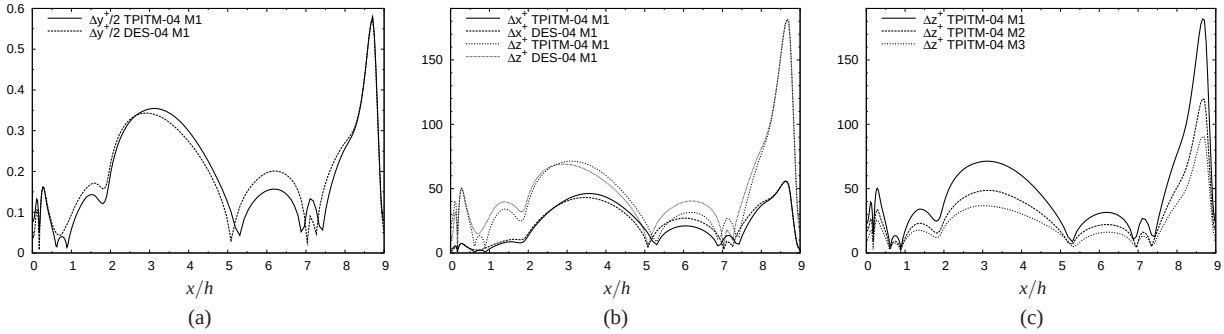

Figure 1: Size of the wall-adjacent cells in wall units along the bottom wall.

the two models provide very similar results, which is an indirect confirmation of the theoretical equivalence established by Manceau et al. (2010). In particular, although reattachment is slightly too late, its location is much better predicted than with the TPITM-02 (*i.e.*, with $\beta_0 = 0.2$) and SST (2D) models (see table 1). Except near the reattachment region (within the range $x/h = 4-6$), the shear stress shown in figure 5 is well predicted by the optimal hybrid models, which prevents the steep velocity profile observed in both SST and TPITM-02 predictions.

The "observed" energy ratio r is shown in Fig. 6. It can be seen that, at the wall, although the computation are in RANS mode, r goes to zero, because of the wrong asymptotic behaviour of the modelled turbulent energy provided by the SST model. Consequently, using r as an indicator of the energy partitioning between resolved and modelled scales is meaningful only outside of the near-wall region. Here, a significant difference between the TPITM and DES approaches can be identified: in the centre of the channel, modelled scales contribute to 30% of the total turbulent energy for the TPITM ($\beta_0 = 0.4$), and only to 10% in DES. The effective control of the amount of modelled energy through the parameter β_0 is also demonstrated. Decreasing this values to $\beta_0 = 0.2$ increases the modelled contribution to around $50-60$%, which degrades the model predictions.

Interestingly, the distribution of the time-averaged function $\overline{\beta^*}$ (Eq. 14) in the TPITM approach, shown in figure 7, provides a good picture of the energy partition in the whole domain. High values correspond to the RANS mode, and low values to the LES mode. When $\beta_0 = 0.2$ is used (Fig. 7a), a substantial portion of the central domain is computed in nearly RANS mode, while $\beta_0 = 0.4$ (Fig. 7b) allows a larger part of the separated shear layer and reversed flow to be computed in LES mode. The influence of the blending function F_2, used in both the approaches to "protect" the boundary layer from the limiters (Eqs. 14 and 15) by enforcing the RANS mode ($F_2 = 1$ – upper limit), deserves to be mentioned. Figure 8 shows the contours of the time-averaged functions F_1 and F_2. These may be regarded as an a-posteriori (qualitative) indication on how the energy parameter ratio $r^{observed}$ in Eq. 14 is affected through the computational domain. Note that $\overline{F_1}$ need to be viewed with caution as it is not effectively used to this purpose. In the TPITM computations (8b and 8d), it can be observed that F_2 is active in a substantial portion

of the domain, even well outside the near-wall region, especially for $\beta_0 = 0.2$. This is not the case in the DES model (Fig. 8f). These observations are consistent with the predictions discussed above. Figure 8c suggests that F_1 would be a more adequate function in the TPITM approach, leading to promising capabilities.

SUMMARY

The *Temporal Partially-Integrated Transport Model* approach, which is based on a consistent formalism for seamless hybrid temporal LES/RANS methodologies was exploited to derive a two-equation subfilter model. The $k-\omega$ SST model was selected as the RANS underlying model due to its reasonably accurate performances in engineering practice. The resulting hybrid model was subjected to a complex flow configuration involving separation from a curved surface. The predictive capabilities of the model was demonstrated in terms of mean-flow topology, shear-stress level and flexibility in controling the amount of the modelled energy. It was also found that the model is comparable with an equivalent DES formulation, when the optimal calibration constants are used. Finally, from these developments, improved modelling proposals may be formulated, for instance, through a better control of the energy partitioning. This route is under inverstigation.

ACKNOWLEDGMENT

This work was granted access to the HPC resources of IDRIS under the allocation 2010-020912 made by GENCI (Grand Equipement National de Calcul Intensif).

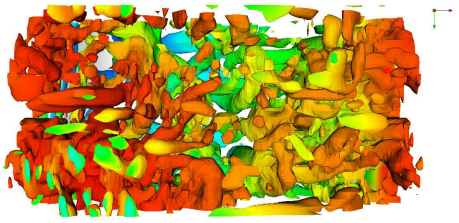

(a) $C_{des} = 0.4$

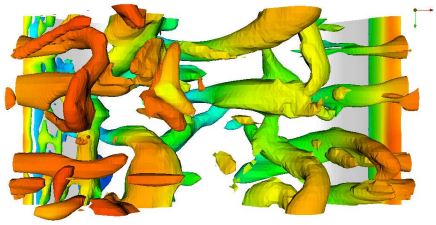

(b) $C_{des} = 0.5$

Figure 2: Isocontour $Q = -\frac{1}{2}\frac{\partial \overline{u_i}}{\partial x_j}\frac{\partial \overline{u_j}}{\partial x_i} = 0.2$ – View from the top – Grid M1.

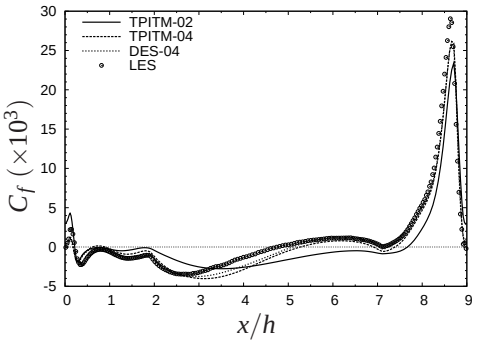

Figure 3: Skin-friction coefficient along the bottom wall – Grid M1.

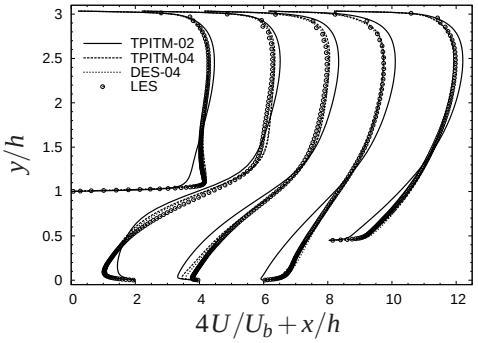

Figure 4: Streamwise velocity profiles – Grid M1.

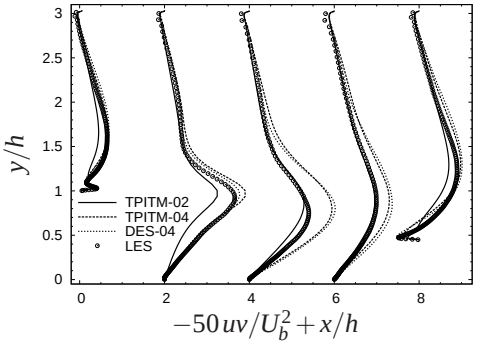

Figure 5: Shear stress profiles – Grid M1.

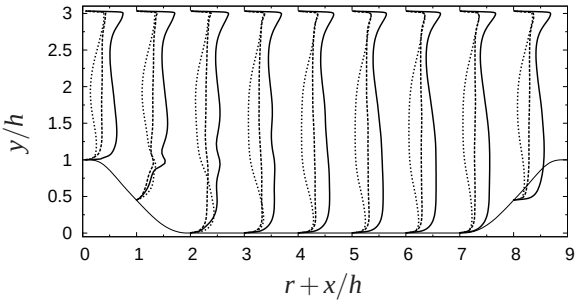

Figure 6: Ratio of modelled energy – Grid M1 (for legend see previous figure).

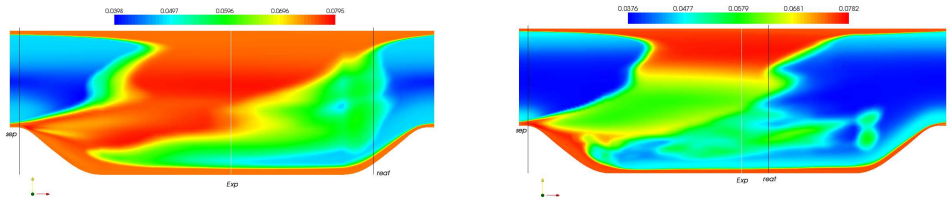

(a) $\beta_0 = 0.2$ (b) $\beta_0 = 0.4$

Figure 7: Contours of the time-averaged function $\overline{\beta^*}$ (see Eq. 14) in the TPITM approach – Grid M1.

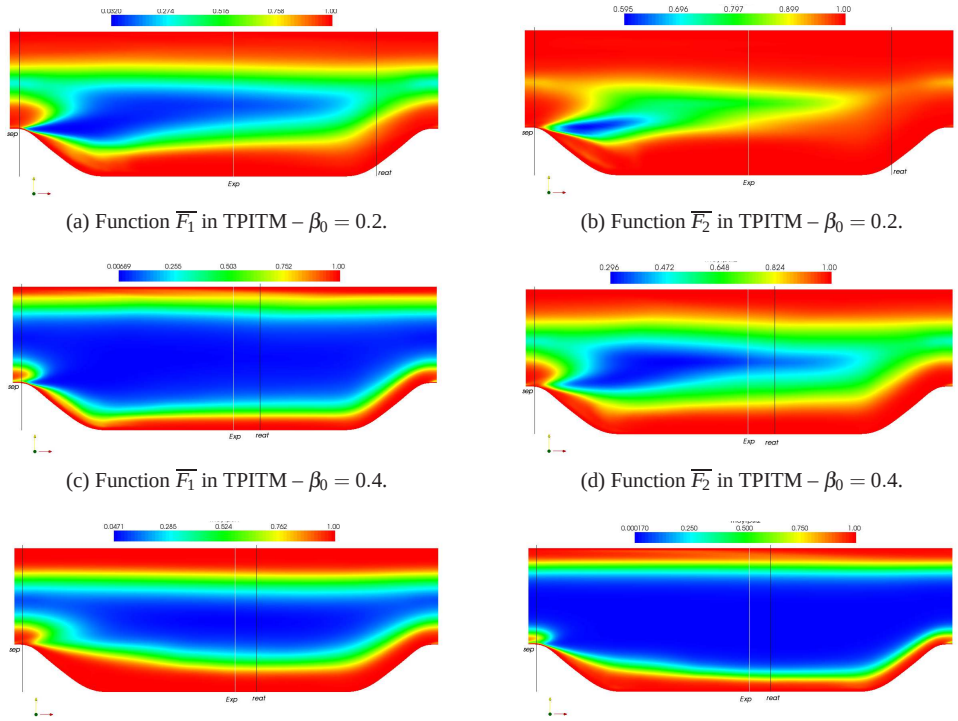

(a) Function $\overline{F_1}$ in TPITM – $\beta_0 = 0.2$. (b) Function $\overline{F_2}$ in TPITM – $\beta_0 = 0.2$.

(c) Function $\overline{F_1}$ in TPITM – $\beta_0 = 0.4$. (d) Function $\overline{F_2}$ in TPITM – $\beta_0 = 0.4$.

(e) Function $\overline{F_1}$ in DES – $C_{des} = 0.4$. (f) Function $\overline{F_2}$ in DES – $C_{des} = 0.4$.

Figure 8: Contours of the time-averaged blending functions $\overline{F_1}$ and $\overline{F_2}$ (Eqs. 6 – 9) – Grid M1.

REFERENCES

F. Archambeau, N. Méchitoua, and M. Sakiz. Code saturne: a finite volume code for the computation of turbulent incompressible flows – industrial applications. *Int. J. Finite Volumes*, 1(1), 2004.

A. Fadai-Ghotbi, C. Friess, R. Manceau, and J. Borée. A seamless hybrid RANS–LES model based on transport equations for the subgrid stresses and elliptic blending. *Phys. Fluids*, 22(5), 2010a.

A. Fadai-Ghotbi, C. Friess, R. Manceau, T. Gatski, and J. Borée. Temporal filtering: A consistent formalism for seamless hybrid RANS–LES modeling in inhomogeneous turbulence. *Int. J. Heat Fluid Flow*, 31:378–389, 2010b.

J. Froehlich, C.P. Mellen, W. Rodi, L. Temmerman, and M. Leschziner. Highly resolved large-eddy simulation of separated flow in a channel with streamwise periodic constrictions. *J. Fluid Mech.*, 526:19–66, 2005.

T. B. Gatski, C. L. Rumsey, and R. Manceau. Current trends in modeling research for turbulent aerodynamic flows. *Phil. Trans. R. Soc. A*, 365(1859):2389–2418, 2007.

M. Germano. Turbulence: the filtering approach. *J. Fluid Mech.*, 238:325–336, 1992.

R. Manceau, C. Friess, and T.B. Gatski. Of the interpretation of DES as a hybrid RANS/Temporal LES method. *Proc. 8th ERCOFTAC Int. Symp. on Eng. Turb. Modelling and Measurements, Marseille, France*, 2010.

F.R. Menter, M. Kuntz, and R. Langtry. Ten Years of Industrial Experience with the SST Turbulence Model. *Turbulence, Heat and Mass Transfer*, 4, 2003.

R. Schiestel and A. Dejoan. Towards a new partially integrated transport model for coarse grid and unsteady turbulent flow simulations. *Theoret. Comput. Fluid Dynamics*, 18:443–468, 2005.

H. Tennekes. Eulerian and Lagrangian time microscales in isotropic turbulence. *J. Fluid Mech.*, 67:561–567, 1975.